

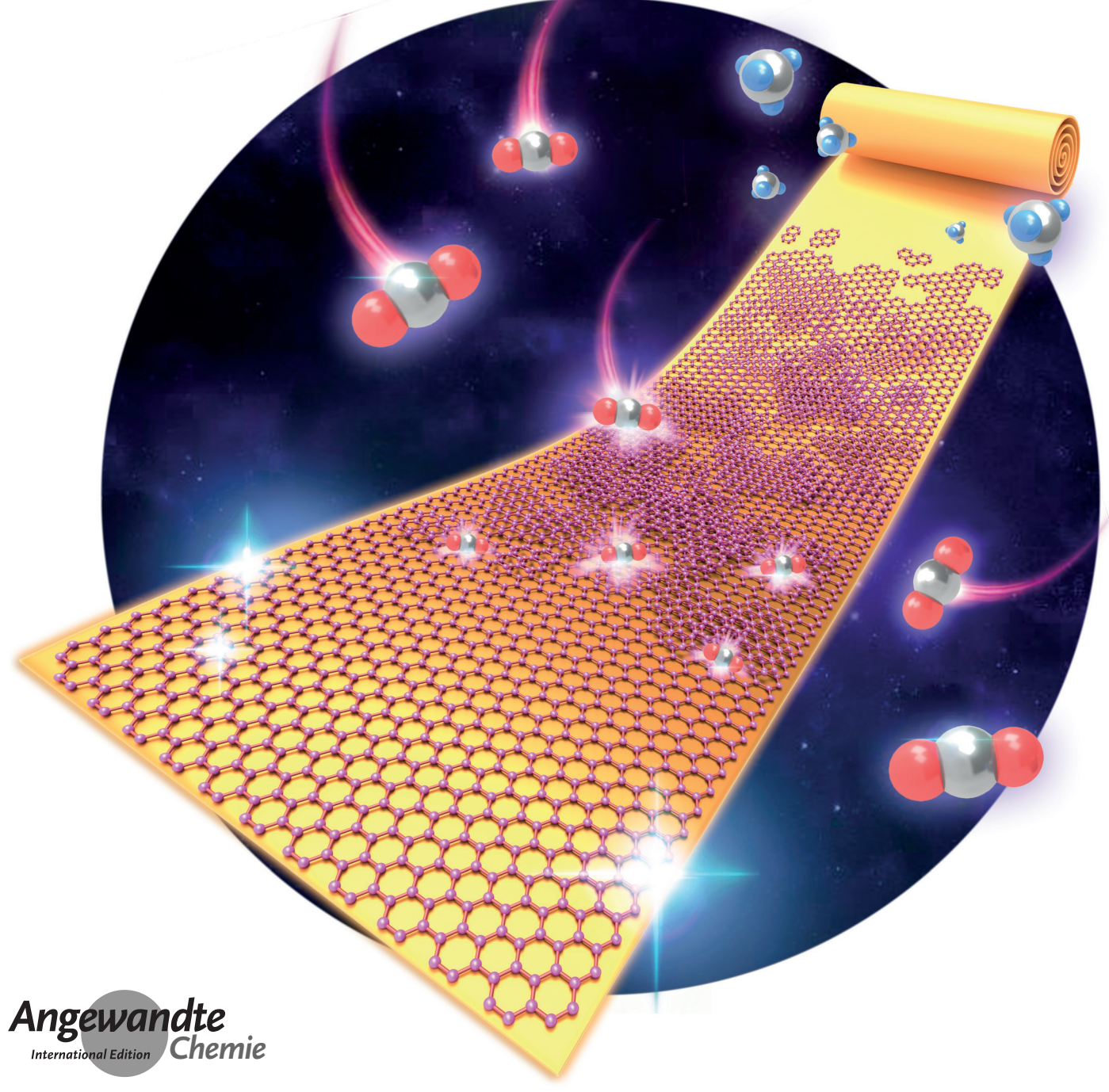


Graphene

International Edition: DOI: 10.1002/anie.201905672 German Edition: DOI: 10.1002/ange.201905672

Large-Area Synthesis of Superclean Graphene via Selective Etching of Amorphous Carbon with Carbon Dioxide

Jincan Zhang⁺, Kaicheng Jia⁺, Li Lin⁺, Wei Zhao, Huy Ta Quang, Luzhao Sun, Tianran Li, Zhenzhu Li, Xiaoting Liu, Liming Zheng, Ruiwen Xue, Jing Gao, Zhengtang Luo, Mark H. Rummeli, Qinghong Yuan, Hailin Peng,* and Zhongfan Liu*



Abstract: Contamination commonly observed on the graphene surface is detrimental to its excellent properties and strongly hinders its application. It is still a great challenge to produce large-area clean graphene film in a low-cost manner. Herein, we demonstrate a facile and scalable chemical vapor deposition approach to synthesize meter-sized samples of superclean graphene with an average cleanness of 99%, relying on the weak oxidizing ability of CO2 to etch away the intrinsic contamination, i.e., amorphous carbon. Remarkably, the elimination of amorphous carbon enables a significant reduction of polymer residues in the transfer of graphene films and the fabrication of graphene-based devices and promises strongly enhanced electrical and optical properties of graphene. The facile synthesis of large-area superclean graphene would open the pathway for both fundamental research and industrial applications of graphene, where a clean surface is highly needed.

Chemical vapor deposition (CVD) has proven to be a promising approach for the industrial production of graphene films^[1] with fine scalability,^[2] controllability,^[3] and uniformity.[4] However, surface contamination on the graphene basal plane is one of long-standing issues^[5,6] that degrade the quality^[7,8] of CVD-grown graphene film and hinder its applications.^[9,10] For instance, the presence of contamination would cause severe scattering of carriers, [8] resulting in a reduced carrier mobility.[11] Contaminations have also been widely reported to strongly alter the surface properties of graphene.^[12] Furthermore, a clean surface is a prerequisite for many promising applications of graphene, including graphene-based electronic and photonic devices^[13,14] and high-resolution transmission electron microscopy (HRTEM) imaging. [15] Consequently, the preparation of clean graphene films on a large scale and at low cost is of great interest for the graphene community.

In the past years, many strategies have been developed to reduce surface contamination with an emphasis on the transfer process, [6,14] among which post-treatment methods such as ultra-high-vacuum annealing, [5,16] post-adsorption, [17] and plasma etching^[18–19] are widely reported. Unfortunately,

these methods usually require a high energy input and suffer from the inevitable introduction of defects in graphene, which in turn strongly degrade the quality of graphene. [16,20] A facile and scalable method to prepare clean and defect-free graphene films without impeding the quality of graphene is still currently in its infancy.

Amorphous carbon introduced during the high-temperature CVD growth process has been reported recently to be another primary origin of surface contamination. [21,22] Herein, based on this, we describe an efficient route to synthesize submeter-long samples of defect-free, superclean graphene by using CO₂ as a mild etchant to selectively eliminate intrinsic contamination, i.e., amorphous carbon (Figure 1 a and Figures S1 and S2). We found that the availability of superclean graphene surfaces ensures a significant reduction of polymer residues after the transfer of graphene onto functional substrates. Furthermore, the elimination of amorphous carbon and transfer-related polymer residues collaboratively contributes to enhanced optical and electrical properties, which would certainly widen the avenues towards graphenebased applications in the future.

The synthesis of superclean graphene consists of the hightemperature growth of graphene at 1020°C and subsequent removal of amorphous carbon with the assistance of CO₂ at ≈ 500 °C (Figure 1 a). During high-temperature growth, amorphous carbon ($\approx 0.3-3$ nm thick) with a dense distribution is formed on graphene surface (Figure S3), and the area ratio of unclean regions is higher than 50% (Figure 1b and Figure S4). The atomic arrangement and bonding structure of amorphous carbon was revealed by HRTEM, where a fast Fourier transform (FFT) mask filter was used to remove the graphene lattice beneath the amorphous carbon (Figure S5).[23] The carbon-carbon bond lengths of amorphous carbon are revealed to range from 0.09 nm to 0.22 nm (Figure S6), and bond angles range from 90° to 150° (Figure 1c). In contrast, the carbon-carbon bond length and bond angle are 0.142 nm and 120°, respectively, in the perfect hexagonal arrangement of carbon atoms in the graphene lattice. This observation indicates the presence of abundant defects with distorted hexagonal, heptagonal, and pentagonal

[*] J. Zhang, [+] K. Jia, [+] L. Lin, [+] L. Sun, T. Li, X. Liu, L. Zheng, H. Peng,

Center for Nanochemistry, Beijing Science and Engineering Center for Nanocarbons, Beijing National Laboratory for Molecular Sciences, College of Chemistry and Molecular Engineering, Peking University

Beijing 100871 (P. R. China) E-mail: hlpeng@pku.edu.cn zfliu@pku.edu.cn

J. Zhang,[+] L. Sun, X. Liu

Academy for Advanced Interdisciplinary Studies, Peking University Beijing 100871 (P. R. China)

W. Zhao, Q. Yuan

State Key Laboratory of Precision Spectroscopy School of Physics and Material Science, East China Normal

Shanghai 200062 (P. R. China)

H. T. Quang, M. H. Rummeli

IFW Dresden, D-01171 Dresden (Germany)

Z. Li, J. Gao, M. H. Rummeli

Soochow Institute for Energy and Materials InnovationS Soochow University, Suzhou 215006 (P. R. China)

Department of Chemical and Biomolecular Engineering Hong Kong University of Science and Technology Clear Water Bay, Hong Kong, SAR 999077 (P. R. China)

M. H. Rummeli

Centre of Polymer and Carbon Materials, Polish Academy of Sciences M. Curie-Sklodowskiej 34, Zabrze 41-819 (Poland)

H. Peng, Prof. Dr. Z. Liu

Beijing Graphene Institute, Beijing 100095 (P. R. China)

[+] These authors contributed equally to this work.

Supporting information (including the synthesis, transfer, charac-

terization of graphene, and computational details) and the ORCID identification number(s) for the author(s) of this article can be found

https://doi.org/10.1002/anie.201905672.

3213773, 2019, 41, Downloaded from https://onlinelibrary.wiley.com/doi/10.1002/anie.201905672 by Socchow University, Wiley Online Library on [15/11/2024]. See the Terms and Conditions (https://onlinelibrary.wiely.com/terms-and-conditions) on Wiley Online Library for rules of use; OA arctices are governed by the applicable Creative Commons License

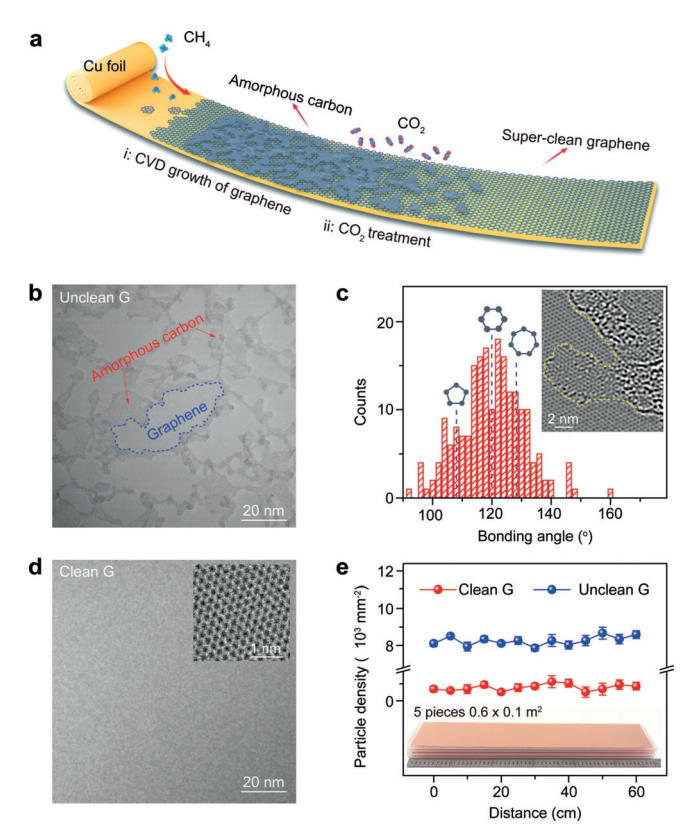


Figure 1. CO₂-assisted preparation of superclean graphene. a) Schematic illustration of the formation and elimination of amorphous carbon contamination on graphene surface during CVD process. b) TEM image of a typical CVD-grown graphene surface. c) C-C bond angle distribution in amorphous carbon regions after removal of the underlying graphene lattice by using a FFT mask filter. Inset: HRTEM image of the clean and contaminated regions with atomic resolution. d) TEM image of a clean graphene surface prepared using CO2 treatment process. Inset: HRTEM image of the clean graphene with atomic resolution. e) Density of TiO2 nanoparticles on clean (red) and unclean (blue) graphene surfaces. Inset: Photograph of five 0.6 × 0.1 m²-sized samples of clean graphene film after TiO₂ visualization.

structures in the amorphous carbon contamination. These defects in amorphous carbon may result in an enhanced reaction activity, in comparison with defect-free graphene basal plane.

After graphene growth, the introduction of CO₂ into the CVD chamber at ≈ 500 °C is proven to initiate the elimination of amorphous carbon from the graphene surface through the reaction: $CO_{2+}C \rightarrow 2CO$, leaving graphene intact (Figures S7-S11). Clean graphene film without defects in the basal plane was observed after the removal of surface contamination, which indicates CO₂ is an efficient etchant for selective removal of amorphous carbon at ≈500°C (Figure 1d and Figures S8, S10, and S11). Meanwhile, a large-area, clean graphene film was successfully prepared in a 6-inch-sized quartz tube, indicating the scalability of our CO2 posttreatment process (inset of Figure 1e). The cleanness of the as-prepared graphene films on Cu foil can be quickly evaluated on a large scale by exposure of the as-synthesized graphene/Cu to TiCl4 vapor in humid air, where lightscattering TiO2 nanoparticles would selectively adsorb on the contaminated regions.^[21,24] Clearly, fewer TiO₂ nanoparticles deposited on CO2-treated graphene surface, in contrast to the densely distributed TiO2 nanoparticles on the graphene surface without CO₂ treatment (Figure 1 e and Figure S12), confirming the improved cleanness of graphene after the CO₂ etching process.

The moderate oxidizing ability of CO₂ is the key factor for the selective etching of amorphous carbon by CO₂. Density functional theory (DFT) calculations were carried out to gain a better understanding of the selective etching capability of CO₂. We used the commonly observed defective structures, such as 5-8-5, 55-77, and 555-777 topological defects as the simplified structures of amorphous carbon in our DFT simulation, based on the HRTEM images of the contamination. The dissociation of CO2 molecules on the surface of amorphous carbon or graphene is the first step for the reaction of CO₂ etching. To fulfill this, the physically adsorbed CO2 molecules must be transformed into the chemically adsorbed CO₂ molecules. In this regard, the reaction barriers for the adsorption and dissociation of CO₂ on the 5-8-5 defect (2.52 eV) are much lower than that on graphene (4.76 eV) (Figure 2a). Reaction barriers of CO₂ dissociation on nanocarbon structures with other kinds of defects are all lower than that on the graphene surface (Figure 2b and Figure S13), confirming that the presence of defects in amorphous carbon is mainly responsible for the easy dissociation of CO₂ molecules. The dissociation rate constants (k) were estimated using the Arrhenius equation [Eq. (1)],

$$k = A e \left((-E_a)/R T \right) \tag{1}$$

in which A is the pre-exponential factor, E_a is the calculated reaction barrier, R is the universal gas constant, and T is the temperature. The rate of the reaction of CO₂ with defective graphene is much faster than that with perfect graphene (Figure 2c). In addition, treatment temperatures ranging from 400 to 550°C were optimal to guarantee the high etching rate of amorphous carbon and avoid the etching of graphene (Figure S6). In contrast, another common oxidizing gas, O2, which has a stronger oxidizing ability, introduces quantities of defects by reaction with graphene, as indicated by TEM and Raman characterization (Figure S14). The ready etching of perfect graphene by O2 is confirmed by the low etching reaction barrier of 2.56 eV, which would result in a relatively low selectivity for the etching reaction (Figure S15).

Graphene grown on metal foil typically needs to be transferred onto functional substrates for further applications, and polymer film such as polymethyl methacrylate (PMMA) usually functions as the transfer medium. Traditionally, the complete removal of polymer is difficult, resulting in a great deal of polymer residue on the surface of the transferred graphene. Interestingly, we found that the elimination of amorphous carbon ensures a significant reduction in the amount of polymer residue left on the graphene surface in the transfer step, i.e., the amount of polymer residue depends directly on the cleanness of the fresh graphene films on Cu foil (Figure S16). A high density of polymer residue is clearly

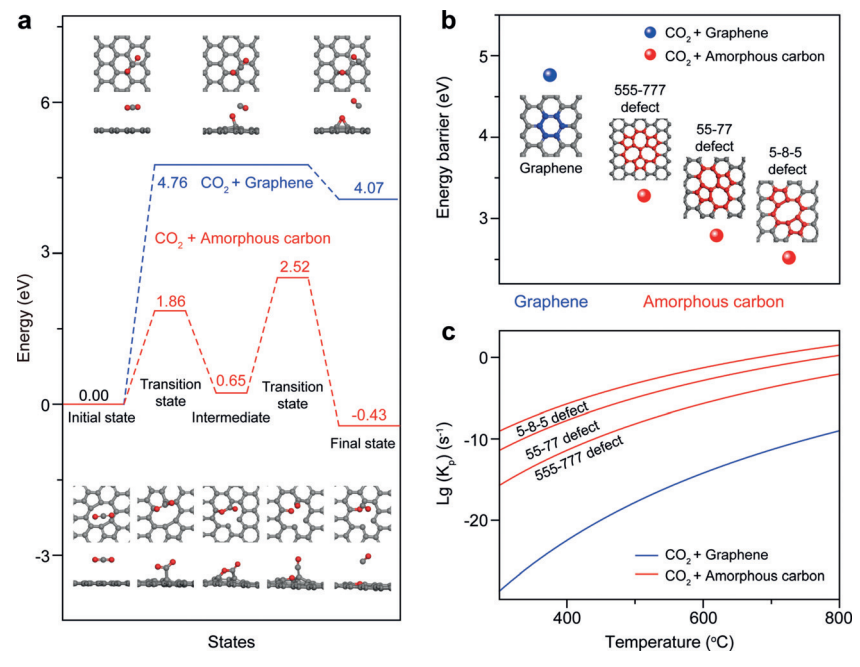


Figure 2. Theoretical exploration of the mechanism of the selective etching of amorphous carbon by CO2. a) Energy profiles of CO2 etching of amorphous carbon (red) and graphene (blue). b) Comparison of energy barriers for the CO2 etching of graphene (blue) and amorphous carbon (red). c) Reaction rates for the CO2 etching of graphene (blue) and amorphous carbon (red). Note that 5-8-5, 555-777, and 55-77 topological defects are taken as simplified model structures of the amorphous carbon contamination.

visible on untreated graphene samples (Figure 3a). In contrast, almost no polymer residue remained on as-transferred clean graphene synthesized via CO2 treatment, as evidenced by the smooth surface and low surface roughness in the AFM image (≈ 0.076 nm per μ m²) (Figure 3b). We also transferred graphene onto SiO₂/Si substrates using ²H-PMMA and utilized ToF-SIMS to detect the amount of ²H⁻ in the transferred graphene; this can reflect the amount of PMMA residue. The ToF-SIMS spectra revealed a strong ²H⁻ signal on transferred graphene samples without CO₂ treatment, confirming the presence of PMMA residues (Figure 3c). In contrast, the intensity of the ²H⁻ signal on transferred clean graphene film was at the noise level. Meanwhile, the high lateral resolution intensity mapping with vertical resolution of ²H⁻ and C⁻ ions of transferred clean and unclean graphene films (Figure 3d and Figure S17) further verified that the amount of polymer residue on clean graphene was significantly less than that on unclean graphene.

The large-scale preparation of graphene film with improved optical and electrical properties is essential for applications of graphene, for example, as transparent conductive films. In this regard, the light transmittance of asobtained clean graphene was found to be higher than that of the unclean counterpart, with a value approximately equal to the theoretical calculation result (Figure 4a and Figure S18), presumably owing to the elimination of amorphous carbon and polymer residue. The decrease of the optical transmittance of unclean graphene is more obvious in the shortwavelength regions: in comparison to its clean counterpart, the optical transmittance of unclean graphene is as low as 0.8% at 550 nm and $\approx 3\%$ at 300 nm (Figure S18c). Moreover, the bi- and trilayer graphene films fabricated via layerby-layer transfer also showed increased optical transmittance (Figure 4a). The improved optical transmittance is also confirmed by in situ contrast spectra measurement, in which the contrast spectrum of clean graphene is comparable to that of mechanically exfoliated graphene (Figure 4b and Figure S19). Meanwhile, the CO₂-treated large-area graphene film showed good electrical conductivity with an average sheet resistance value of $\approx 390 \ \Omega \, \text{sq}^{-1}$, extracted from hundreds of Hall bar devices fabricated on a 4-inch SiO₂/Si wafer (Figure 4c). Similar reduction of sheet resistance was observed in graphene transferred onto flexible plastic substrates (Figure S20), indicating the potential of as-obtained clean graphene film for future applications in the field of large-area flexible electronics.

We have demonstrated a facile posttreatment method for preparing largearea, superclean graphene films, assisted by the selective etching of amorphous carbon by CO2. Meanwhile, polymer residue after the transfer of graphene onto

functional substrates was significantly reduced on the clean graphene surface. The reduction of surface contamination contributed to the improved optical and electrical properties of graphene. Our results provide a new pathway for future graphene research and industrial applications, such as electrical and optoelectronic devices and organic light-emitting diodes.

Acknowledgements

We thank Lutao Weng at the Hong Kong University of Science and Technology for help with ToF-SIMS characterization and discussion. We thank Liang Zhao for help during HRTEM characterization. We also thank Beijing National Laboratory for Molecular Science. This work was financially supported by the Beijing Municipal Science & Technology Commission (No. Z181100004818001), the National Basic Research Program of China (No. 2016YFA0200101), the National Natural Science Foundation of China (Nos. 21525310, 51432002, and 51520105003).

Conflict of interest

The authors declare no conflict of interest.

Keywords: carbon dioxide · chemical vapor deposition ·

graphene · selective etching

15213773, 2019, 41, Downloaded from https://onlinelibrary.wiley.com/doi/10.1002/anie.201905672 by Socchow University, Wiley Online Library on [15/11/2024]. See the Terms and Conditions (https://onlinelibrary.wiley.com/terms-and-conditions) on Wiley Online Library for rules of use; OA arcicles are governed by the applicable Creative Commons License

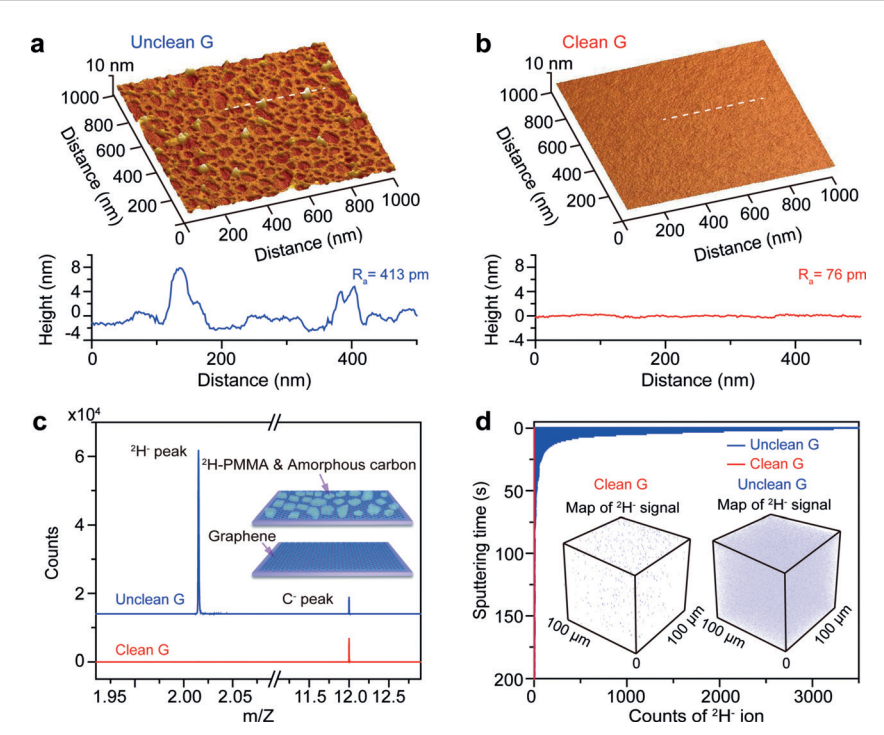


Figure 3. Decreased amounts of polymer residue on clean graphene surface. a,b) Atomic force microscopy (AFM) images of transferred unclean (a) and clean graphene (b) on SiO_2/Si substrates and the height profiles of the marked lines. c) Time-of-flight secondary-ion mass spectrometry (ToF-SIMS) spectra of transferred clean (red) and unclean graphene (blue) on SiO_2/Si substrates after removal of 2 H-labeled marked PMMA (2 H-PMMA), using the same transfer process. Inset: Schematic of the cleanness-dependent amount of polymer residue on a transferred graphene surface. d) Depth profiles of 2 H- for clean (red) and unclean (blue) graphene films transferred onto SiO_2/Si substrates after removal of 2 H-PMMA. Inset: ToF-SIMS maps of the three-dimensional distribution of secondary-ion 2 H- on transferred clean (left) and unclean (right) graphene. Note that the size of the mapping regions is $100 \times 100 \ \mu m^2$ and the sputter time is kept the same at 300 s.

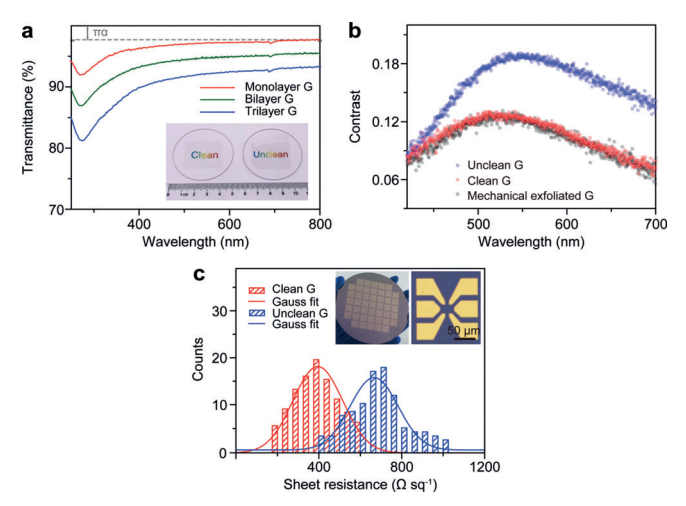


Figure 4. Improved optical and electrical properties of clean graphene. a) UV/Vis spectra of monolayer (red), bilayer (green), and trilayer (blue) superclean graphene films on quartz substrates. Inset: Photograph of transferred clean (left) and unclean (right) monolayer graphene films on quartz substrates 5 cm in diameter. b) Contrast spectra of as-prepared clean (red) and unclean (blue) graphene films and mechanically exfoliated monolayer graphene (black) on 90 nm SiO_2/Si substrates as a function of wavelength. c) Statistics of the sheet resistance of clean (red) and unclean (blue) graphene devices. Inset: Photograph of wafer-sized graphene devices fabricated using a lithography technique (left) and optical microscopy image of a typical graphene Hall bar device (right).

How to cite: Angew. Chem. Int. Ed. **2019**, 58, 14446–14451 Angew. Chem. **2019**, 131, 14588–14593

- [1] K. S. Novoselov, V. I. Fal'ko, L. Colombo, P. R. Gellert, M. G. Schwab, K. Kim, *Nature* 2012, 490, 192–200.
- [2] S. Bae, H. Kim, Y. Lee, X. Xu, J. S. Park, Y. Zheng, J. Balakrishnan, T. Lei, H. R. Kim, Y. I. Song, Y. J. Kim, K. S. Kim, B. Ozyilmaz, J. H. Ahn, B. H. Hong, S. Iijima, *Nat. Nanotechnol.* 2010, 5, 574–578.
- [3] Z. Yan, Y. Liu, L. Ju, Z. Peng, J. Lin, G. Wang, H. Zhou, C. Xiang, E. L. Samuel, C. Kittrell, V. I. Artyukhov, F. Wang, B. I. Yakobson, J. M. Tour, Angew. Chem. Int. Ed. 2014, 53, 1565–1569; Angew. Chem. 2014, 126, 1591–1595.
- [4] Y. F. Hao, M. S. Bharathi, L. Wang, Y. Y. Liu, H. Chen, S. Nie, X. H. Wang, H. Chou, C. Tan, B. Fallahazad, H. Ramanarayan, C. W. Magnuson, E. Tutuc, B. I. Yakobson, K. F. McCarty, Y. W. Zhang, P. Kim, J. Hone, L. Colombo, R. S. Ruoff, *Science* 2013, 342, 720–723.
- [5] Y. C. Lin, C. C. Lu, C. H. Yeh, C. Jin, K. Suenaga, P. W. Chiu, Nano Lett. 2012, 12, 414–419.
- [6] S. J. Kim, T. Choi, B. Lee, S. Lee, K. Choi, J. B. Park, J. M. Yoo, Y. S. Choi, J. Ryu, P. Kim, J. Hone, B. H. Hong, *Nano Lett.* 2015, 15, 3236–3240.
- [7] M. T. Pettes, I. S. Jo, Z. Yao, L. Shi, Nano Lett. 2011, 11, 1195– 1200.
- [8] J. H. Chen, C. Jang, S. D. Xiao, M. Ishigami, M. S. Fuhrer, *Nat. Nanotechnol.* 2008, 3, 206–209.
- [9] H. Hong, J. C. Zhang, J. Zhang, R. X. Qiao, F. R. Yao, Y. Cheng, C. C. Wu, L. Lin, K. C. Jia, Y. C. Zhao, Q. Zhao, P. Gao, J. Xiong, K. B. Shi, D. P. Yu, Z. F. Liu, S. Meng, H. L. Peng, K. H. Liu, J. Am. Chem. Soc. 2018, 140, 14952–14957.

Communications





- [10] D. Yang, R. X. Yang, S. Priya, S. Z. Liu, Angew. Chem. Int. Ed. 2019, 58, 4466-4483; Angew. Chem. 2019, 131, 4512-4530.
- [11] K. I. Bolotin, K. J. Sikes, Z. Jiang, M. Klima, G. Fudenberg, J. Hone, P. Kim, H. L. Stormer, Solid State Commun. 2008, 146, 351 - 355.
- [12] Z. Li, Y. Wang, A. Kozbial, G. Shenoy, F. Zhou, R. McGinley, P. Ireland, B. Morganstein, A. Kunkel, S. P. Surwade, L. Li, H. Liu, Nat. Mater. 2013, 12, 925-931.
- [13] Y. Kim, S. S. Cruz, K. Lee, B. O. Alawode, C. Choi, Y. Song, J. M. Johnson, C. Heidelberger, W. Kong, S. Choi, K. Qiao, I. Almansouri, E. A. Fitzgerald, J. Kong, A. M. Kolpak, J. Hwang, J. Kim, Nature 2017, 544, 340-343.
- [14] Z. Zhang, J. Du, D. Zhang, H. Sun, L. Yin, L. Ma, J. Chen, D. Ma, H. M. Cheng, W. Ren, Nat. Commun. 2017, 8, 14560.
- [15] C. J. Russo, L. A. Passmore, Nat. Methods 2014, 11, 649-652.
- [16] M. Tripathi, A. Mittelberger, K. Mustonen, C. Mangler, J. Kotakoski, J. C. Meyer, T. Susi, Phys. Status Solidi RRL 2017, 11, 1700124.
- [17] J.-N. Longchamp, C. Escher, H.-W. Fink, J. Vac. Sci. Technol. B **2013**, 31, 020605.
- [18] G. Cunge, D. Ferrah, C. Petit-Etienne, A. Davydova, H. Okuno, D. Kalita, V. Bouchiat, O. Renault, J. Appl. Phys. 2015, 118,

- [19] Y. D. Lim, D. Y. Lee, T. Z. Shen, C. H. Ra, J. Y. Choi, W. J. Yoo, ACS Nano 2012, 6, 4410-4417.
- [20] J. Wu, L. Xie, Y. Li, H. Wang, Y. Ouyang, J. Guo, H. Dai, J. Am. Chem. Soc. 2011, 133, 19668-19671.
- [21] L. Lin, J. C. Zhang, H. S. Su, J. Y. Li, L. Z. Sun, Z. H. Wang, F. Xu, C. Liu, S. Lopatin, Y. H. Zhu, K. C. Jia, S. L. Chen, D. R. Rui, J. Y. Sun, R. W. Xue, P. Gao, N. Kang, Y. Han, H. Q. Xu, Y. Cao, K. S. Novoselov, Z. Q. Tian, B. Ren, H. L. Peng, Z. F. Liu, Nat. Commun. 2019, 10, 1912.
- [22] K. C. Jia, J. C. Zhang, L. Lin, Z. Z. Li, J. Gao, L. Z. Sun, R. W. Xue, J. Y. Li, N. Kang, Z. T. Luo, M. H. Rummeli, H. L. Peng, Z. F. Liu, J. Am. Chem. Soc. 2019, 141, 7670-7674.
- [23] K. Kim, Z. Lee, W. Regan, C. Kisielowski, M. F. Crommie, A. Zettl, ACS Nano 2011, 5, 2142-2146.
- [24] R. Zhang, Y. Zhang, Q. Zhang, H. Xie, H. Wang, J. Nie, Q. Wen, F. Wei, Nat. Commun. 2013, 4, 1727.

Manuscript received: May 7, 2019 Revised manuscript received: June 23, 2019 Accepted manuscript online: July 8, 2019 Version of record online: August 7, 2019